

# Application of scatterometry-based machine learning to control multiple electron beam lithography

AM: Advanced Metrology

Nivea Figueiro, Francisco Sanchez, Roy Koret,  
Michael Shifrin, Yoav Etzioni, Shay Wolfling,  
Matthew Sendelbach  
Nova Measuring Instruments  
Rehovot, Israel  
nivea-f@novameasuring.com

Yoann Blancquaert, Thibault Labbaye,  
Guido Rademaker, Jonathan Pradelles, Lucie  
Mourier, Stephane Rey, Laurent Pain  
CEA-LETI, Minatec Campus  
Grenoble, France  
yoann.blancquaert@cea.fr

**Abstract** – The evaluation of scatterometry and machine learning for the monitoring of intended critical dimension (CD) variations within scatterometry targets is presented. Such variations mimic non-uniformities potentially caused by massively parallel e-beam Maskless Lithography (ML2). Although previous results [1] demonstrate that traditional model-based scatterometry can properly quantify these within-target variations, the current work shows that the application of scatterometry-based machine learning complements the model-based scatterometry results. While model-based scatterometry can provide information about structure profile, which can be used to detect parameter shifts even in the absence of a reference, machine learning provides superb correlation to a defined reference.

**Keywords**—*machine learning, scatterometry, alternative lithography, e-beam lithography, multibeam, multiple e-beam, dose variation, TMU, TMU analysis*

## I. INTRODUCTION

In recent years, several different patterning methods have been developed to overcome traditional photolithography limitations, including Extreme Ultraviolet Lithography (EUVL), Directed Self-Assembly (DSA), Nanoimprint Lithography (NIL), Sidewall Image Transfer (SIT) and e-beam Maskless Lithography (ML2). Regarding the last technique, massively parallel e-beam direct write has recently started to demonstrate advanced patterning capability. But full adoption of any such patterning methods must include the development of metrology and inspection techniques that can meet the specified requirements for production monitoring and control.

For multibeam Maskless Lithography, beam-to-beam variation can consist of changes or differences in beam dose or focus [2]. In order to monitor and eventually control such variations, a non-destructive, high throughput, precise, and accurate metrology method is required. Scatterometry is a commonly used manufacturing metrology method used to measure periodic structures; however, it has also been shown to measure patterning variation levels of non-periodic structures [3]. This ability to quickly and inexpensively detect and quantify undesired, non-periodic variations across large regions makes scatterometry appealing for such applications. Previous work [1] has already demonstrated the success of scatterometry

in measuring defects in patterning caused by simulated dose variations in multibeam Maskless Lithography. The measured parameter is called the effective CD, which is the average CD across a grating of lines with regions of POR (Process of Record) CD and intentionally non-POR CD, weighted by the areas of those regions.

## II. MACHINE LEARNING

The present work extends and improves upon this by applying machine learning methods to quantify CD variations, including the effective CD, caused by beam-to-beam dose shifts. Machine learning [4] is the application of Artificial Intelligence (AI) methods to provide systems the ability to predict outcomes by themselves based on some type of training.

In order to implement a machine learning solution, training and validation steps must be performed. For the training step, a set of signals and their corresponding values are paired. These corresponding values are collected by a reference tool, independently from the signals, and are called the reference values or reference data. The data pairs (each signal and its reference value) are input into the machine learning algorithm, which then “learns” how to accept other signals (similar, but not necessarily identical, to those used in the training step) and outputs associated values that closely match what the reference tool would have provided. The system is said to be “trained” so that the input signals are linked to the reference metrology. A machine learning solution is thus generated from this training process. In the validation step, signals are input into the machine learning solution. The output results are compared to known reference results in order to confirm a good correlation. In this work, the machine learning methodology used is called “scatterometry-based” because scatterometry spectra are the input signals.

## III. STRUCTURE AND DESIGN

In this work the film stack of the measured structures consists of a patterned e-beam resist on top of an Anti-Reflective Coating and a Spin-on Carbon (SoC) hard mask (Fig. 1). Two wafers were patterned and measured. The first was used in the previous work [1] from this project, while the second was produced more recently using a different lithography process

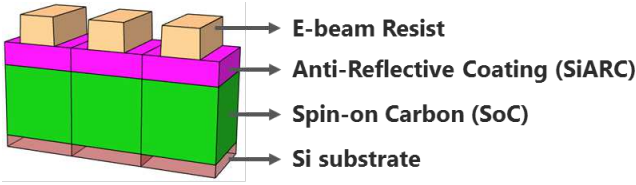


Fig. 1. Film stack used in this work.

and printed with targets designed differently than the first wafer. The measurement structures for both wafers consisted of line/space arrays and were patterned using a Variable Shaped Beam tool in a manner to mimic how a multibeam tool at CEA-LETI [5, 6] might pattern a wafer.

### A. First Wafer Design

For the first wafer, this mimicking was done by exposing each  $50 \times 50 \mu\text{m}$  scatterometry target in 25 stripes, each  $2 \mu\text{m}$  wide and  $50 \mu\text{m}$  long. The intentional dose variations, used to change line CDs, are implemented within the targets. The eight rows (labeled 0 – 7) indicate the number of e-beams, each responsible for patterning a  $2 \mu\text{m}$  wide strip, within the target that have a magnitude shift in dose. The three columns indicate the magnitude of the dose shift, nominally measured in nm (2, 5, 10 nm). The row 0 target is exposed in a POR manner and so has no dose-shifted region. Fig. 2 shows the specially-designed scatterometry targets used for this wafer, and also, in order to better understand how intentional dose shifts were incorporated into the targets, shows how the targets in row 7 were exposed. These targets mimic the shift in dose of the center 7 beams, totaling a shifted region that is  $14 \mu\text{m}$  wide through the target’s center. The first wafer contained 9 die that were measured, all of which were exposed in a nominally identical manner.

### B. Second Wafer Design

For the second wafer, the mimicking was done by exposing each  $100 \times 100 \mu\text{m}$  target in 50 stripes, each  $2 \mu\text{m}$  wide and  $100 \mu\text{m}$  long. For non-POR targets, the intentional CD changes are manifested in either 1, 3, or 6 of the 50 stripes (target types L1, L3, and L6). For target types L3 and L6, adjacent non-POR stripes are separated by a single stripe with POR dose. Non-POR targets have magnitudes of nominal line CD shifts in non-POR stripes ranging from 2 nm to 15 nm. This wafer’s target designs are shown in Fig. 3. A sample CD-SEM image from a portion of one of the non-POR targets is shown in Fig. 4. The image shows part of a non-POR region (smaller line CD) in between POR regions (larger line CD).

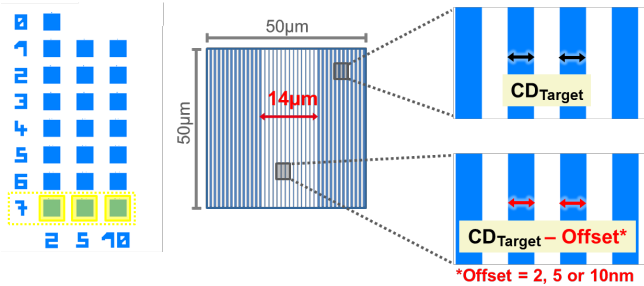


Fig. 2. Scatterometry target array (left) for the first wafer. This set of targets is copied 9 times across the wafer. The targets in row 7 have seven  $2 \mu\text{m}$ -wide stripes ( $14 \mu\text{m}$  in total width) that were exposed with a non-POR dose.

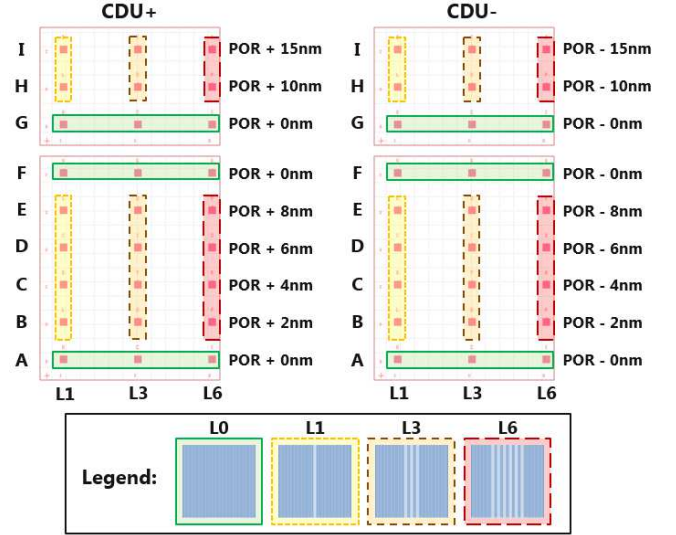


Fig. 3. Scatterometry target design for the second wafer. There are 18 POR targets, each exposed at the POR dose (L0, highlighted in green in rows A, F, and G). The rest of the targets each have either 1, 3, or 6 stripes exposed at the non-POR dose (target types L1, L3, and L6). All targets are  $100 \times 100 \mu\text{m}$ . The horizontal axis for the target schematics in the legend is not to scale.

The second wafer contained 13 measured die. Nine of these (“POR die”) were exposed in a nominally identical manner, while the other 4 (“DOE die”) were exposed so that the baseline dose (the dose of the POR regions of the targets) was varied relative to the baseline dose of the other 9 die, causing changes in baseline CD. The CD shifts from POR shown in Fig. 3 are relative to the baseline CD of the die in question.

## IV. TMU ANALYSIS AND SAMPLING

### A. Overview of TMU Analysis

In this work, TMU (Total Measurement Uncertainty) analysis is used to assess the measurement quality of the scatterometry and machine learning solutions relative to a defined reference. TMU analysis [7, 8, 9] was originally developed to be a type of calibration exercise where measurements from a Tool under Test (TuT) could be calibrated to those of a Reference Measurement System (RMS). Its most common use now, however, is to assess both relative accuracy and precision by combining them into a single meaningful metric. Here, relative accuracy is defined as the ability of one measurement method to track changes in a measured parameter when compared to another measurement method, while being insensitive to changes in other parameters and unaffected by the average offset between the methods.

TMU analysis computes the total error (scatter) in a correlation between measurements from the TuT and the RMS, and states that this total error is the sum of two terms, one of which is associated with the TuT and the other is associated with all other errors. The  $3\sigma$  form of the errors associated with the TuT is given by:

$$TMU \equiv 3 \sqrt{\hat{\sigma}_{Mandel}^2 - \frac{RMSU^2}{9}} \quad (1)$$

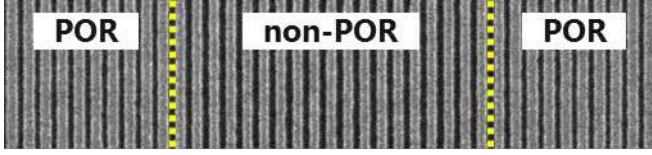


Fig. 4. A sample CD-SEM image from a portion of a non-POR target. The smaller line CD of the non-POR region is clearly evident. The width of the non-POR region is 2  $\mu\text{m}$  (1 beam).

where  $\hat{\sigma}_{Mandel}^2$  is the total error in variance form (also called the Mandel variance) and RMSU (Reference Measurement System Uncertainty) is the  $3\sigma$  form of the compilation of all other errors, most notably those errors associated with the RMS. The “hat” symbol over the sigma indicates that this is an estimated quantity. Although other quantities are also estimated, such as TMU and RMSU, for brevity purposes they are not given “hat” symbols. Besides the TMU and slope of the best-fit line, another important metric in TMU analysis is the average offset:

$$\text{average offset} \equiv \bar{x} - \bar{y} \quad (2)$$

where  $\bar{x}$  is the average of the TuT measurements and  $\bar{y}$  is the average of the RMS measurements.

### B. Advantages of TMU Analysis

Different methods are used among semiconductor metrologists to determine accuracy, but one of the most common methods is Ordinary Least Squares (OLS) regression, where the accuracy metric is  $R^2$ . TMU analysis has many advantages over OLS regression and the  $R^2$  metric, including the use of units in TMU analysis. Having an accuracy metric with units matching those of the measurement parameter makes it easy to apply specifications (specs). TMU analysis also is not nominally affected by the range of the data, so comparisons across different data sets and applications are straightforward. TMU analysis takes into account the error of the RMS. This is not done with OLS regression, yet in the semiconductor industry the RMS can often be a significant contributor to the scatter when compared to the TuT. Finally, TMU analysis computes meaningful upper and lower confidence limits. Typically, no confidence limits are calculated with OLS regression.

### C. Reference Metrology Sampling

The RMSU can be calculated in different ways [10], depending primarily on the metrology sampling. Reference [1], however, extends the methodology for calculating RMSU for samples that are nominally non-uniform, like those used here.

The Reference Measurement System for this work is defined to be the critical dimension scanning electron microscope (CD-SEM). The use of “defined” here specifically means that the CD-SEM is merely used as a benchmark against which the scatterometry and machine learning results will be compared, and does not mean that the CD-SEM is a “better” measurement. Thus, the CD-SEM should be thought of more as an independent measurement system to be compared against, and not as the “gold standard” measurement system for this application. This is important to understand when comparing both model-based scatterometry measurements and machine learning measurements of effective CD to the CD-SEM results. The machine learning methods will be shown to have equivalent or

improved correlation to the CD-SEM reference because the machine learning algorithms are designed to do this, regardless of the “actual” accuracy of the reference; the scatterometry measurements, on the other hand, are only indirectly influenced by the reference results (when the model is adjusted to better correlate to the reference values).

As before [1], multiple CD-SEM measurement locations per target are used to calculate the effective CD, some in the non-error regions and some in the error regions (for those targets with error regions). Each location consists of multiple lines measured by the CD-SEM. Because scatterometry measures the average CD across its spot, the average CD from the CD-SEM must properly take into account the contributions from both the non-error and error regions in order for a correct comparison to occur. To do this, the average of the measured CDs from the non-error region ( $\overline{CD}_{NE_{meas}}$ ) and the average of the measured CDs from the error region ( $\overline{CD}_{E_{meas}}$ ) are weighted by area to determine the CD-SEM weighted average CD for the target, which is the CD-SEM’s determination of the effective CD:

$$CD_{Weighted} = \frac{(A_{NE})(\overline{CD}_{NE_{meas}}) + (A_E)(\overline{CD}_{E_{meas}})}{A_{NE} + A_E} \quad (3)$$

where  $A_{NE}$  is the total area of the non-error regions within the scatterometry measurement spot and  $A_E$  is the total area of the error regions within the spot.

## V. RESULTS

### A. First Wafer

In the previous work [1], model-based scatterometry results from POR and non-POR targets on the first wafer were compared to CD-SEM results which were collected from many locations, both POR and non-POR regions of each target, and properly averaged according to the relative areas of the different regions. Initial results (Fig. 5(a)) of this correlation of the effective CD were unexpected (TMU of 3.65 nm), as typical TMU results for this type of application are on the order of 1 nm. Upon investigation, it was discovered that variations in the slope and offset of the best-fit line between scatterometry and CD-SEM for each die were caused by changes in resist morphology due to variation of the resist develop process across the wafer. These changes in resist morphology were significant enough to

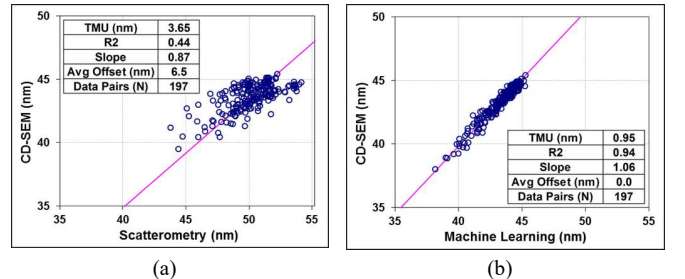


Fig. 5. First wafer effective CD correlation for (a) model-based scatterometry and (b) machine learning, each compared to the CD-SEM (equipment system “1”). The correlation is much better for machine learning, largely because it is not as susceptible as model-based scatterometry to changes in secondary parameters. All nine die and all of the different types of targets on the first wafer are represented.

cause a variation in CD measurement sensitivity between scatterometry and CD-SEM, resulting in the different slopes and offsets. In order to better determine the intrinsic quality of the scatterometry measurement, independent of these effects, the correlations were redone, but instead calculated on a per-die basis. The resulting TMU (and  $R^2$ ) values (Fig. 6, left side) were significantly better, and agreed with expectations.

Since that work, additional analysis of the spectra was done using specialized machine learning algorithms optimized for such spectra, using the CD-SEM for training. Results of the machine learning determination of effective CD show significantly better correlation to CD-SEM for all die together (Fig. 5(b)) as well as improved correlation for the majority of the die when analyzed on a per-die basis (Fig. 6, right side).

### B. Second Wafer: Model-Based Scatterometry

For the second wafer, the targets with 10 and 15 nm nominal CD shifts for their non-POR regions were not included in the model-based scatterometry analysis because the focus of the work was in detecting smaller shifts, and inclusion of larger shifts could impact this sensitivity. Using different target designs and an updated lithography process, the second wafer produced an improved correlation between model-based scatterometry and CD-SEM (Fig. 7) compared to the first wafer. However, the correlation, like in the first wafer, is not as expected and shows structure within the scatter, suggesting systematic effects. Analysis of this scatter by differentiating according to die number (Fig. 8) and number of non-POR beams per target (Fig. 9) reveals structure in both cases. As in the first wafer, die-to-die variation creates best-fit lines with varying slopes and offsets. At least part of this variation is hypothesized to be caused by differences in resist morphology caused by changes in baseline dose that some of the die received. For the differentiation according to the number of non-POR beams, targets L3 and L6 have different slopes compared to L0 and L1. The cause for this is hypothesized to be related to the fact that L3 and L6 have multiple non-POR beams, perhaps causing slight differences in stray electron scattering during exposure that affect resist morphology. In addition, the slightly worse correlation (TMU) for L3 further contributes to the scatter in Fig. 7. One contribution to this observation may be related to how each of the different non-POR targets breaks the periodicity assumption of the scatterometry model. As was done for the first wafer, the correlations were redone using a per-die analysis so that the intrinsic quality of the scatterometry measurement

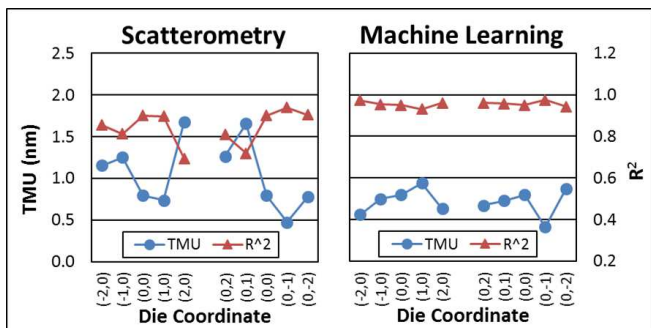


Fig. 6. Scatterometry (left side) and machine learning (right side) vs. CD-SEM for the first wafer – correlation (TMU and  $R^2$ ) results by die.

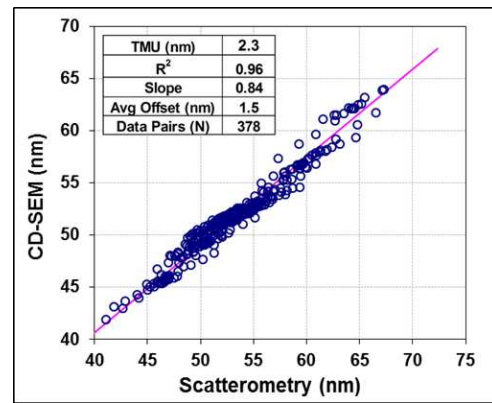


Fig. 7. Second wafer correlation of the effective CD between model-based scatterometry and CD-SEM (equipment system “2”). All 13 die and all of the different types of targets on the second wafer are represented, except for those with a nominal CD shift of 10 or 15 nm.

could be more closely determined. The resulting correlations (Fig 10, left side) were much better.

### C. Second Wafer: Scatterometry-Based Machine Learning

As in the analysis of the model-based scatterometry correlation to CD-SEM, the analysis of the machine learning correlation to CD-SEM for effective CD did not include the targets with 10 and 15 nm nominal CD shifts for their non-POR regions. In this way, the validity of the comparison of both methods to CD-SEM is optimized. Like for the first wafer, the correlation of the machine learning results to those of the CD-SEM (Fig. 11) is improved over the model-based results. Also, the per-die correlations were determined (Fig. 10, right side), and are comparable to the model-based per-die results.

Since scatterometry-based machine learning algorithms can be trained using data that do not correspond to traditional parameters of interest supplied by scatterometry, an investigation was conducted into finding out its effectiveness in determining whether it can detect the presence of non-POR regions of the target. Such a capability could be used as a flag in development or manufacturing for the presence of one or more defective beams. The reason for this is that, up until now,

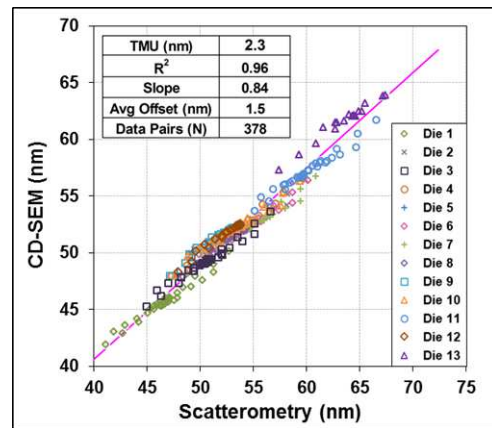


Fig. 8. Second wafer correlation of the effective CD between model-based scatterometry and CD-SEM (equipment system “2”), differentiated by die. The best-fit line and the values in the table are for the entire data set (all die, as in Fig. 7).

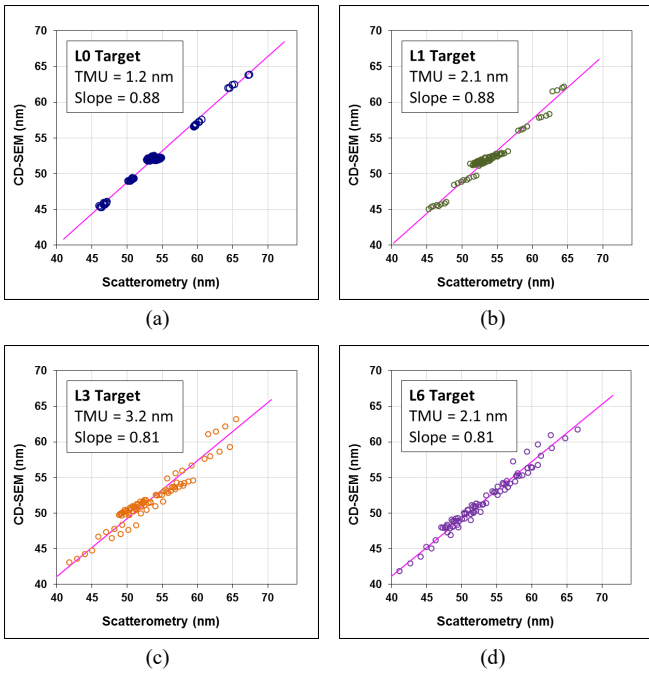


Fig. 9. Second wafer correlation of the effective CD between model-based scatterometry and CD-SEM (equipment system “2”), separated out by target type according to the number of non-POR stripes in the target. The L0 and L1 best-fit line slopes are different than those of L3 and L6, contributing to the overall scatter seen in Fig. 7. The relatively larger scatter that the L3 data have, as measured by TMU, further contributes to the overall scatter in Fig. 7.

the CD measurement methods using scatterometry spectra (whether model-based or machine learning-based) have not been designed to differentiate whether a CD result deviating from the target value is due to fewer deviant beams with a larger dose shift or more deviant beams with a smaller dose shift. Using for training both the number of non-POR stripes in the target and the CD shift of those stripes, the machine learning algorithms were used to develop a solution that could use the scatterometry spectra from a target to measure a factor that is a function of the number of non-POR stripes and the CD shift. Fig. 12(a) shows the correlation of the machine learning measurement to this factor. For this test, targets containing all possible CD shifts shown in Fig. 3 were included; however, only the 9 POR die were used in order to simulate a manufacturing environment in which the baseline dose is tightly controlled, but where small numbers of beams can still have CD shifts relative to the baseline. The TMU of 0.92 (arbitrary units) indicates the

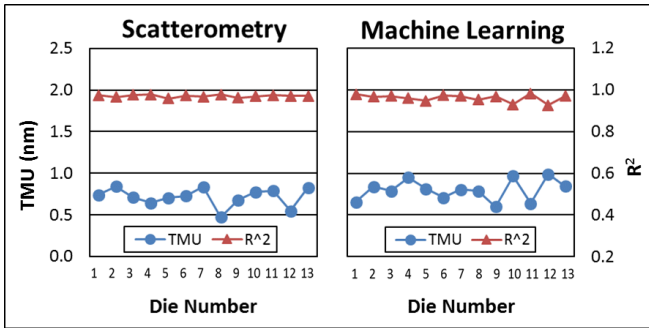


Fig. 10. Scatterometry (left side) and machine learning (right side) vs. CD-SEM for the second wafer – correlation (TMU and  $R^2$ ) results by die.

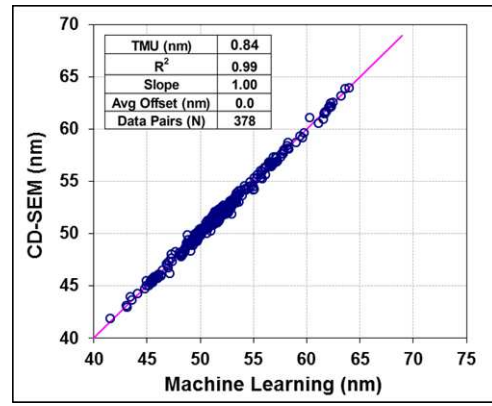


Fig. 11. Second wafer correlation of the effective CD between scatterometry-based machine learning and CD-SEM (equipment system “2”). The correlation is better than that of scatterometry (Fig. 7), largely because machine learning is not as susceptible as model-based scatterometry to changes in secondary parameters. All 13 die and all of the different types of targets on the second wafer are represented, except for those with a nominal CD shift of 10 or 15 nm.

error of the machine learning solution in measuring the factor. For this particular function that was used to calculate the factor, this TMU result means that the solution is sensitive enough to detect the presence of a single non-POR stripe as long as its CD shift is at least 0.9 nm, or two non-POR stripes with CD shifts at least 0.5 nm, or three non-POR stripes with CD shifts at least 0.1 nm. Because TMU is a  $3\sigma$  parameter, the theoretical confidence level of these detection limits is 99.7%.

The next test also used all of the targets shown in Fig. 3. Furthermore, it used the same 9 die used in the previous test, plus the two DOE die that have a baseline dose closest to that of the 9 POR die (a shift in the baseline CD of roughly 5 nm or less). This test simulates a more challenging environment in which the baseline dose (and CD) is less controlled than in the first test, effectively introducing another variable (baseline CD) that affects the spectra. Fig. 12(b) shows the correlation, with a TMU of 2.1 (arbitrary units). In this case, this TMU result corresponds to a solution that is sensitive enough to detect the

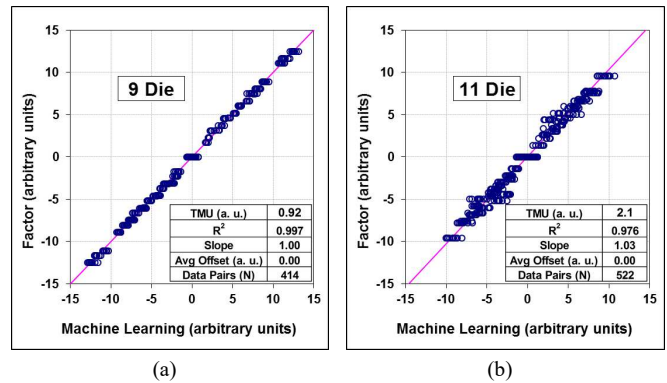


Fig. 12. Second wafer correlation of machine learning results to a factor that is a function of the number of non-POR stripes in the target and the CD shift of those stripes, for both (a) the 9 POR die and (b) the 9 POR die plus 2 of the DOE die. Targets containing all possible CD shifts shown in Fig. 3 were included. Because the TMU represents the  $3\sigma$  error of the machine learning measurement, it can be used to determine the sensitivity of the solution. For the 9 die test, it is sensitive enough to discern a single non-POR stripe with a CD shift as little as 0.9 nm. For the 11 die test, the sensitivity reaches a level of 4 nm for a single non-POR stripe.

presence of a single non-POR stripe with a CD shift of at least 4 nm, or two stripes with a CD shift of 2 nm, or three stripes with a CD shift of 0.8 nm.

## VI. DISCUSSION AND CONCLUSIONS

The support of multiple e-beam Maskless Lithography (ML2) for manufacturing applications requires high throughput, non-destructive, and accurate metrology for the detection of defects specific to this lithography. In this work, defects caused by electron beam-to-beam dose variation were intentionally printed, and then measured using model-based scatterometry, scatterometry-based machine learning, and CD-SEM methods.

Initially, the weighted average CD within the target, or effective CD, was evaluated for scatterometry and machine learning, using CD-SEM as the defined reference. It is noted that CD-SEM is defined as the reference because it is an independent, high throughput, and well understood metrology, but is not necessarily intrinsically more accurate than the other methods. Results reveal that individual per-die correlations of effective CD between scatterometry and CD-SEM are significantly stronger than entire-wafer correlations. It is hypothesized that this is primarily due to the circumvention of across-wafer resist morphology variation effects in the per-die correlations.

The scatterometry-based machine learning measurement of effective CD was trained using the CD-SEM measurement and specialized algorithms. An independent metrology method was needed as the reference in order to demonstrate the capability of machine learning to correlate well to that reference for this non-standard application. Results show that machine learning performed better than scatterometry for correlations using data from the entire wafer because machine learning is much less susceptible (or not susceptible at all) to physical characteristics or anomalies that can affect model-based scatterometry. When such anomalies are minimized, the model-based scatterometry correlations are improved.

As a next step into the machine learning capabilities, an investigation into its ability to flag one or more defective stripes in a target was performed. This ability goes beyond that of measuring effective CD, as the latter cannot differentiate between how many defective stripes are present versus the size of the average CD shift of those stripes. An algorithm was developed that enabled the method to be sensitive to detecting CD shifts less than 1 nm for a single stripe in the target for simulated manufacturing conditions. Thus, machine learning not only demonstrated its ability to measure the effective CD, but also its sensitivity in differentiating a target with very small beam defects from a target with no beam defects.

This work highlights the concept that model-based scatterometry and scatterometry-based machine learning measurements can be used in a complementary manner. Model-based scatterometry does not rely on large amounts of reference data and provides sensitivity to profile information, while machine learning provides a "direct link" to the defined reference (often resulting in better correlation to that reference), insensitivity to other parameters (that often affect model-based scatterometry measurements), and a faster time-to-solution once the reference data is available. Additional research will explore

the use of additional hardware channels as well as the detection of other types of multiple e-beam exposure defects.

## ACKNOWLEDGMENT

The authors would like to thank Mapper Lithography for the valuable technical exchange regarding multibeam equipment.

## REFERENCES

- [1] Y. Blancquaert *et al.*, "Scatterometry control for multiple electron beam lithography", Proc. of SPIE 10145, Metrology, Inspection, and Process Control for Microlithography XXXI, 101451F (28 March 2017); doi: 10.1117/12.2261389.
- [2] P. Brandt *et al.*, "Demonstration of electronic design automation flow for massively parallel e-beam lithography" in J. Micro/Nanolith. MEMS MOEMS 13(3) 031306 (2014) DOI: 10.1117/1.JMM.13.3.031306.
- [3] R. Chao *et al.*, "Scatterometry-based Defect Detection for DSA In-line Process Control", Proc. of SPIE Vol. 9424, 942419-1 (2015); doi: 10.1117/12.2087093.
- [4] T. Hastie, R. Tibshirani, and J. Friedman, *The Elements of Statistical Learning: Data Mining, Inference, and Prediction*, 2nd ed., Springer, 2008.
- [5] G. de Boer *et al.*, "MAPPER: progress toward a high-volume manufacturing system", Proc. of SPIE Vol. 8680, 868000 (2013); doi: 10.1117/12.2011486.
- [6] M. Wieland *et al.*, "Performance validation of Mapper's FLX-1200", Proc. of SPIE Vol. 9423 (2015).
- [7] M. Sendelbach *et al.*, "Effect of measurement error budgets and hybrid metrology on qualification metrology sampling" in J. Micro/Nanolith. MEMS MOEMS 13(4) 041414 (2014) DOI: 10.1117/1.JMM.13.4.041414.
- [8] M. Sendelbach and C. N. Archie, "Scatterometry measurement precision and accuracy below 70 nm", Proc. of SPIE Vol. 5038 (SPIE, Bellingham, WA 2003) pp. 224-238.
- [9] M. Sendelbach, A. Munoz, K. A. Bandy, D. Prager, and M. Funk, "Integrated scatterometry in high-volume manufacturing for polysilicon gate etch control", Proc. of SPIE Vol. 6152 (SPIE, Bellingham, WA 2006) 61520F.
- [10] M. Sendelbach *et al.*, "Feedforward of mask open measurements on an integrated scatterometer to improve gate linewidth control", Proc. of SPIE Vol. 5375 (SPIE, Bellingham, WA 2004) pp. 686-702.